Monte Carlo Simulation Study of the Kinetics of Brush Formation by Irreversible Adsorption of Telechelic Polymers onto a Solid Substrate

ARTICLE *in* LANGMUIR · FEBRUARY 2006

Impact Factor: 4.46 · DOI: 10.1021/la051750v · Source: PubMed

6 AUTHORS, INCLUDING:

Ye Zhang
University of Utah
13 PUBLICATIONS **108** CITATIONS
SEE PROFILE

Dmitry Bedrov
University of Utah
165 PUBLICATIONS **3,157** CITATIONS
SEE PROFILE

Monte Carlo Simulation Study of the Kinetics of Brush Formation by Irreversible Adsorption of Telechelic Polymers onto a Solid Substrate

Grant D. Smith,* Ye Zhang, Fang Yin, and Dmitry Bedrov

Department of Materials Science and Engineering, Department of Chemical Engineering, University of Utah, 122 S. Central Campus Drive, Salt Lake City, Utah 84112

M. D. Dadmun and Zhenyu Huang

Department of Chemistry, University of Tennessee, Knoxville, Tennessee 37996

Received June 29, 2005. In Final Form: October 18, 2005

The irreversible adsorption of telechelic polymer chains from solution and melts onto solid substrates has been studied using the bond fluctuation Monte Carlo model. Complex brush formation kinetics dominated by diffusion of chains to the substrate at short times (diffusion-limited regime or DLR) and by penetration of chains through the maturing brush at longer times (penetration-limited regime or PLR) were observed. During the entire adsorption process, the rate of chain adsorption decreases monotonically with time. In the DLR, characterized by a maximum in the concentration of singly bound chains and a rapidly increasing fraction of doubly bound chains (loops), this decrease is due primarily to the depletion of free chains near the substrate and the formation of concentration gradients of free (nonadsorbed) chains in the bulk solution. The DLR and PLR are separated by an intermediate regime during which the brush becomes dominated by doubly bound chains and both penetration of the maturing brush and diffusion of chains to the brush surface play a role in determining the kinetics of brush growth. The PLR is characterized by steep gradients of free chains within the growing brush and the disappearance of concentration gradients for free chains in the bulk solution. In the PLR, the concentration of singly bound chains is low and decreases slowly while surface coverage and the fraction of doubly bound chains increase slowly. The rates of adsorption of new chains and the formation of loops in the PLR slow dramatically with increasing surface coverage and increasing chain length and less dramatically with decreasing bulk concentration.

I. Introduction

Control of the structure of polymeric interfaces can afford a mechanism to direct the functionality of a material. One common and successful method for modifying an interface of a material is to anchor polymer chains to the surface to change the interfacial structure and its physicochemical properties. When the density of tethered chains is high enough so that neighboring chains overlap, the crowded chains stretch away from the interface, forming a polymer brush.[1−8] This stretched conformation is the defining characteristic of brushes and results in unique aggregation, phase, and dynamic behavior.[9−19] For example, it has been shown that frictional interactions are severely reduced when two brush-covered surfaces are brought into contact and sheared against each other.[14−16] Recent work by Dadmun and co-workers has identified the presence of polymer loops, or chains bound to a surface by both ends, as an effective and efficient method to improve the adhesion between two phases.[20−24] It appears that the presence of the loops provides a structure to which free homopolymers can entangle, forming a strong binding force between the phases. This only occurs when the loops are sufficiently separated to enable this entanglement. Alternatively, as loops become more closely packed on a surface, they begin to behave similarly to a singly end tethered polymer brush, where it is expected that interpenetration between two surfaces covered with loops will be less than that of two polymer brushes. Consequently, the dynamic response of such surfaces could be further enhanced.[25−28]

Unfortunately, no clear method currently exists to reproducibly and controllably create a surface covered by multiply tethered polymer chains, nor have there been any thorough, systematic

* To whom correspondence should be addressed.

(1) Alexander, S. J. *J. Phys.−Paris* **1977**, *38*, 977.
(2) DeGennes, P. G. *J. Phys.−Paris* **1976**, *37*, 1445.
(3) DeGennes, P. G. *Macromolecules* **1980**, *13*, 1069.
(4) Cantor, R. *Macromolecules* **1981**, *14*, 1186.
(5) Milner, S. T.; Witten, T. A.; Cates, M. E. *Europhys. Lett.* **1988**, *5*, 413.
(6) Wijmans, C. M.; Scheutjens, J. M.; Zhulina, E. B. *Macromolecules* **1992**, *25*, 2657.
(7) Field, J. B.; Toprakcioglu, C.; Ball, R. C.; Stanley, H. B.; Dai, L.; Barford, W.; Penfold, J.; Smith, G.; Hamilton, W. *Macromolecules* **1992**, *25*, 434.
(8) Field, J. B.; Toprakcioglu, C.; Dai, L.; Hadziioannou, G.; Smith, G.; Hamilton, W. *J. Phys. II* **1992**, *2*, 2221.
(9) Dong, H.; Marko, F.; Witten, T. A. *Macromolecules* **1994**, *27*, 6428.
(10) Zhulina, E. B.; Balazs, A. C. *Macromolecules* **1996**, *29*, 2667.
(11) Zhulina, E. B.; Singh, C.; Balazs, A. C. *Macromolecules* **1996**, *29*, 8254.
(12) Gersappe, G.; Fasolka, M.; Israels, R.; Balasz, A. C. *Macromolecules* **1995**, *28* 4753.
(13) Chern, S.-S.; Zhulina, E. B.; Pickett, G. T.; Balasz, A. C. *J. Chem. Phys.* **1998**, *108*, 5981.
(14) Klein, J. *J. Annu. Rev. Mater. Sci.* **1996**, *26*, 581.
(15) Klein, J.; Kumacheva, E.; Mahalu, D.; Perahia, D.; Fetters, L. J. *Nature* **1994**, *370*, 634.
(16) Kilbey, S. M.; Watanabe, H.; Tirrell, M. *Macromolecules* **2001**, *34*, 5249.
(17) Grest, G. S.; Murat, M. In *Monte Carlo and Molecular Dynamics Simulations in Polymer Science*; Binder, K., Ed.; Oxford University Press: London, 1995.
(18) Chidambaram, S.; Dadmun, M. D. *Comput. Theor. Polym. Sci.* **1999**, *9*, 47.
(19) Taunton, H. J.; Toprakcioglu, C.; Fetters, L. J.; Klein, J. *Nature* **1988**, *332*, 712.
(20) Dadmun, M. D. *Macromolecules*, **1996**, *29*, 3868.
(21) Dadmun, M. D. *Computational Studies, Nanotechnology, and Solution Thermodynamics of Polymer Systems*; Kluwer Academic: New York, 2000; p 69.
(22) Eastwood, E.; Dadmun, M. D. *Macromolecules* **2002**, *35*, 5069.
(23) Eastwood, E.; Dadmun, M. D. *Polymer* **2002**, *43*, 6707.
(24) O′Brien, C.; Rice, J. K.; Dadmun, M. D. *Eur. Polym. J.* **2004**, *40*, 115.
(25) Klein, J. *J. Phys: Condens. Matter* **2000**, *12*, A19-A27.
(26) DeGennes, P. G. *J. Phys.−Paris* **1975**, *36*, 1199.
(27) Klein, J. *Macromolecules* **1986**, *19*, 105.
(28) DeGennes, P. G. *Molecular Conformation and Dynamics of Macromolecules in Condensed Systems*; Elsevier: Amsterdam, 1988.

10.1021/la051750v CCC: $33.50
Published on Web 12/17/2005

studies of structure−property relationships of such modified surfaces. Collaborative experimental and computational programs are underway to develop this understanding. In this paper, our goal is to utilize molecular simulations to gain insight into the kinetics and structure of brushes formed by irreversible adsorption of telechelic polymers from melt and solution onto solid substrates. Since telechelic chains are functionalized at both ends, these chains can in principle be doubly bound to a substrate where strong attractive interactions or chemical reaction between the end groups and the substrate occur. In this paper, we concentrate on understanding the kinetics of brush formation as a function of length of the telechelic chains and concentration of telechelic chains in the solution in contact with the substrate.

II. Simulation Methodology

The bond-fluctuation Monte Carlo (BFMC) simulation method has been used extensively in simulations of the structure and dynamics of polymer solutions,[29] polymer melts,[30] and polymers at solid substrates,[31] including polymeric brushes.[32−43] Two of the latter studies[42,43] involve investigation of equilibrium conformations and dynamics of double-tethered polymers at an impenetrable interface but did not address issues of the kinetics of brush formation that is the primary goal of the present study.

The BFMC model utilizes a coarse-grained lattice representation of polymer chains where a lattice monomer represents several chemical repeat units. A detailed description of the model and methodology can be found in ref 44. In the BFMC method, each lattice monomer occupies a cubic unit of eight lattice sites. Monomers in a polymer are connected by one of 108 bond vectors of the set P(2,0,0), P(2,1,0), P(2,1,1), P(2,2,1), P(3,0,0), and P(3,1,0), where P denotes all permutations and sign combinations. In other words, monomers are connected by bond vectors with lengths 2, $\sqrt{5}$, $\sqrt{6}$, 3, or $\sqrt{10}$ l, where l is the lattice spacing. The movement of monomers or chains includes local monomer moves and slithering snake moves (used only in early stage of equilibration).[45] For each trial move, the randomly selected monomer (or end group of a chain if in slithering snake moves) will move randomly along $\pm x$, $\pm y$, or $\pm z$ by a distance of l. If the new bond is one of the 108 allowed bonds and the new position is empty, the new configuration will be accepted. Otherwise, this trial move fails and a new monomer will be randomly selected to repeat the above process.

The primary advantages of the BFMC model are its computational expediency resulting from the simple structure of the polymers, simple, short-range form of the interactions between monomers (excluded volume) and the discretized nature of inter-

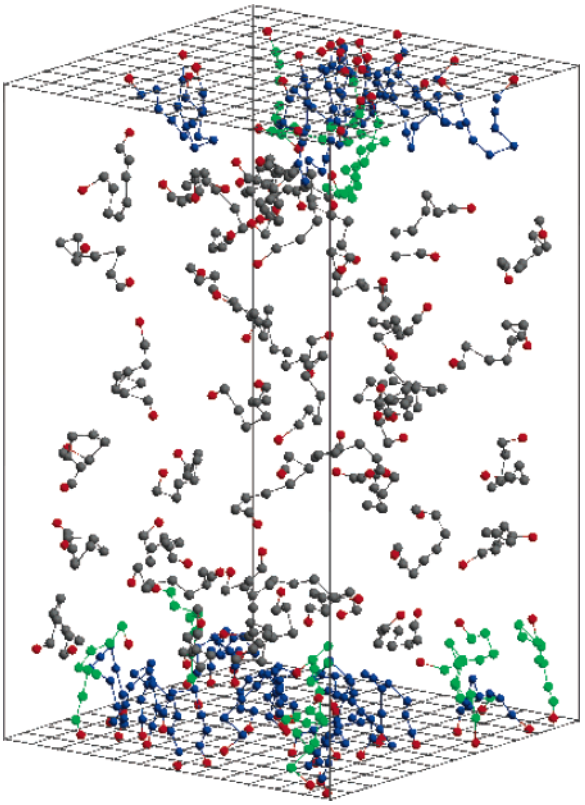

Figure 1. Snapshot from a BFMC simulation of a $\rho_{bulk} = 0.5$, $L = 10$ system. Red monomers are reactive end-groups, whereas gray, green, and blue monomers are central monomers of free, singly bound, and doubly bound chains, respectively. Note that only 20% of the chains in the system are shown for clarity.

monomer distance due to the lattice and the well-established ability of the model to capture the scaling behavior of the structure and dynamics of polymer chains. The primary limitations are lack of chemical specificity and inability to describe subsegmental properties, inability to capture hydrodynamic interactions in polymer solutions and unrealistically large compressibility at densities commonly considered to represent dense polymer melts. Despite these limitation, comparison of polymer dynamics in polymer blends, solutions and melts[46−48] obtained from BFMC simulation with experiment provide satisfying agreement.

A. Description of Systems Simulated. In our model, ensembles of BFMC chains are confined between two parallel flat, impenetrable substrates as illustrated in Figure 1. The maximum occupancy of the system is one monomer per 8 cubic lattice units ($8l^3$). For each system the substrates consisted of 48 × 48 lattice units. Three chain lengths comprised of $L = 10$, 20, and 40 monomers per chain and three concentrations (densities) $\rho_{bulk} = 0.10$, 0.25, and 0.50 for each chain length were investigated. The bulk density is determined as the fraction of maximum occupancy, e.g., $\rho_{bulk} = 0.10$ corresponds to 0.10 monomer/$8l^3$. A density $\rho_{bulk} = 0.50$ is commonly considered to represent a dense polymer melt. The number of telechelic chains was chosen such that there are twice as many chain ends in the simulation cell as surface sites. Importantly, and in contrast to previous simulation studies,[35] this leads to a large excess of chains in the system such that the adsorption kinetics are not strongly influenced by depletion of chains. Parameters and

(29) Paul, W.; Binder, K.; Heermann, D. W.; Kremer, K. *J. Non-Cryst. Solids* **1991**, *131−133* (Pt. 2), 650.
(30) Lobe, B.; Baschnagel, J.; Binder, K. *J. Non-Cryst. Solids* **1994**, *172−174* (Pt. 1), 384.
(31) Baschnagel, J.; Binder, K. *Macromol. Theory Simul.* **1996**, *5*, 417.
(32) Lai, P.-Y.; Binder, K. *J. Chem. Phys.* **1991**, *95*, 9288.
(33) Lai, P.-Y.; Binder, K. *J. Chem. Phys.* **1993**, *98*, 586.
(34) Lai, P.-Y.; Binder, K. *J. Chem. Phys.* **1993**, *98*, 2366.
(35) Lai, P.-Y. *J. Chem. Phys.* **1993**, *98*, 669.
(36) Wittmer, J.; Johner, A.; Joanny, J.-F.; Binder, K. *J. Chem. Phys.* **1994**, *101*, 4379.
(37) Binder, K.; Lai, P.-Y.; Wittmer, J. *Faraday Discuss. Chem. Soc.* **1994**, *98*, 97.
(38) Wittmer, J.; Johner, A.; Joanny, J.-F. *Colloids Surf. A: Physicochem. Eng. Aspects* **1994**, *1*, 37.
(39) Kopf, A.; Baschnagel, J.; Wittmer, J.; Binder, K. *Macromolecules* **1996**, *29*, 1433.
(40) Huh, J.; Balazs, A. C. *J. Chem. Phys.* **2000**, *113*, 2025.
(41) Chen, C.-M.; Fwu, Y.-A *Phys. Rev. E* **2000**, *63*, 011506−1.
(42) Gulati, H. S.; Hall, C. K., Jones, R. L.; Spontak, R. J. *J. Chem. Phys.* **1996**, *105*, 7712.
(43) Jones, R. L.; Spontak, R. J. *J. Chem. Phys.* **1995**, *103*, 5137.
(44) Carmesin, I.; Kremer, K. *Macromolecules* **1988**, *21*, 2819.
(45) Wall, F. T.; Mandel, F. J. *Chem. Phys.* **1975**, *63*, 4592.
(46) Kamath, S.; Colby, R. H.; Kumar, S. K. *Macromolecules* **2003**, *36*, 8567−8573
(47) Di Cecca, A.; Freire, J. J. *Macromolecules* **2002**, *35*, 2851−2858.
(48) Paul, W.; Smith, G. D. *Rep. Prog. Phys.* **2004**, *67*, 1117−1185.

Table 1. Properties of the Telechelic Systems

ρ_{bulk}[a] (l^{-3})	L (l)	Z (l)	number of chains	$\langle b_l \rangle$[b] (l)	R_g[c] (l)	$1/R_g^2$ (l^{-2})	R_e[d] (l)	τ_c[e] (MCS)
0.10	10	400	1152	2.69	4.06	0.061	9.92	1150
	20	800	1152	2.69	6.21	0.026	15.39	5960
	40	1600	1152	2.69	9.28	0.012	23.02	29730
0.25	10	160	1152	2.67	3.90	0.066	9.48	1540
	20	320	1152	2.67	5.87	0.029	14.31	8050
	40	640	1152	2.67	8.61	0.013	21.07	39860
0.50	10	80	1152	2.60	3.67	0.074	8.78	3910
	20	160	1152	2.61	5.41	0.034	13.09	20080
	40	320	1152	2.60	7.83	0.016	19.11	84240

[a] $\rho_{bulk} = 1$ corresponds to a completely filled lattice (1 monomer/$8l^3$). [b] R.M.S bond length. [c] R.M.S. radius of gyration. [d] R.M.S. end-to-end distance. [e] End-to-end vector autocorrelation time.

properties of the telechelic polymer systems simulated are listed in Table 1.

Beginning with random placement of the chains, equilibration of the systems was carried out in two stages. The first stage consisted of both local monomer displacements and slithering snake moves at a ratio of 1:1. In other words, in every Monte Carlo step (MCS) each chain will on average make a slithering snake movement attempt once and each monomer will on average make a local displacement attempt once during the first stage. After an arbitrary time of 10^5 MCS the second stage consisting of only local monomer displacements was initiated. Starting from the second stage of equilibration, every MCS consists of (on average) one local displacement attempt for each monomer. The systems were equilibrated for 10−50 chain end-to-end vector autocorrelation times (see Table 1) during the second stage. Multiple starting configurations for simulations of the adsorption process (see below) were obtained from the original equilibrated systems by running successively for 10−50 autocorrelation times. Properties of the equilibrated systems are described in Table 1.

B. Simulation of the Irreversible Adsorption Process. After equilibration the irreversible adsorption process was simulated as follows. Whenever either "reactive" end group of a telechelic chain contacts the substrate during the BFMC simulation, which involves only monomer displacement moves (no slithering snake moves), it is consider adsorbed and is not allowed to move further. The kinetics of chain adsorption were collected based upon a large number of independent runs that were generated from the equilibrated configurations (one adsorption run per equilibrated configuration) as described above. The number of configurations utilized in our study of adsorption kinetics ranged from 40 for collecting short-time ($<10^4$ MCS) statistics to 20 for long-time ($>10^4$ MCS) statistics. Each simulated configuration provide two sets of data corresponding to the two impenetrable substrates ($z = 1$ and $z = Z$, see Figure 1).

C. Maximum Surface Coverage. The number of adsorbed chain ends per unit surface area (in units l^{-2}) is given the symbol σ_{occ}. Full occupancy of the substrate corresponds to σ_{occ} (full) $= \sigma_{full} = 0.25$, as each adsorbed end group occupies four lattice sites on the substrate. To determine the maximum realizable surface coverage simulations of a system of monomers (i.e., $L = 1$) were carried out at various ρ_{bulk} where each monomer is "reactive" to the substrate. Simulations of the monomer solutions for 2×10^7 MCS yielded a maximum realizable coverage of σ_{occ} (maximum) $= \sigma_{max} = 0.1875 \pm 0.0125$ independent of ρ_{bulk}. A value $\sigma_{max} = 0.20$ was utilized in analysis of the penetration-limited regime described in section V.

D. Brush Density Profile. We will consider the structural properties of the adsorbed telechelic brushes in detail in a future paper. However, to facilitate understanding of the kinetics of brush formation, it is useful to consider the time evolution of the brush density profile. The brush density profile is determined by monitoring the positions of all monomers comprising chains that are adsorbed (singly or doubly bound) to the substrate. Averaging over time is performed on a logarithmic basis. For example, $\langle t \rangle = 5 \times 10^5$ MCS (see Figure 2) is the average over all profiles corresponding to $1 \times 10^5 < t \leq 1 \times 10^6$ MCS. The brush density profile is given by

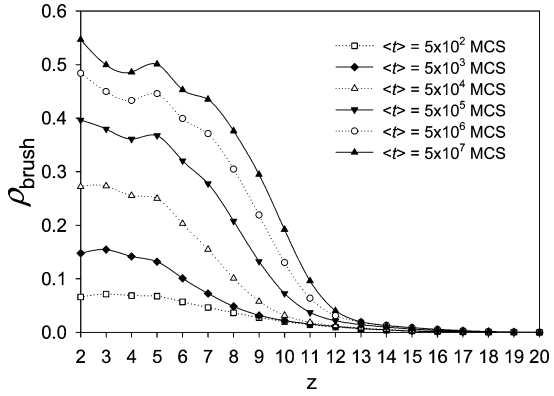

Figure 2. Time evolution of the brush density profile for the $\rho_{bulk} = 0.10$, $L = 10$ system.

$$\rho_{brush}(z, \langle t \rangle) = N(z, \langle t \rangle)/(48 \times 48 \times 2) \quad (1)$$

where $N(z, \langle t \rangle)$ is determined by counting number of occupied sites (note that each monomer occupies eight sites) within the two layers adjacent to z and averaging over all runs and the time range corresponding to $\langle t \rangle$. The evolution of the brush density profile for a representative system is shown in Figure 2. During the adsorption process the brushes are initially sparse, i.e., $\sigma_{occ} < 1/R_g^2$ (see Table 1), and exhibit density profiles typical of the mushroom regime.[49] As the brushes mature overlap of chains occurs ($\sigma_{occ} > 1/R_g^2$) and brushes exhibit profiles typical of moderately stretched chains.[49] Note however that the density profiles do not change dramatically in shape during the adsorption process for accessible adsorption times nor do the brush heights increase dramatically.

III. Kinetic Regimes of Chain Adsorption

We consider brush formation to be describable by two irreversible reactions

$$\text{free} + \text{s} \xrightarrow{k_{sgl}} \text{sgl} \quad (2a)$$

$$\text{sgl} + \text{s} \xrightarrow{k_{dbl}} \text{dbl} \quad (2b)$$

where free, sgl, and dbl indicate free (nonbound), singly bound, and doubly bound chains (loops), s indicates a free (available) surface site for end group adsorption and k_{sgl} and k_{dbl} are reaction rate constants. In the first reaction singly bound chains are formed while in the second they are consumed to form loops. The number of singly bound and doubly bound polymer chains per unit surface area (l^{-2}), σ_{sgl} and σ_{dbl}, respectively, are shown as a function of time (MCS) in Figure 3 (a,b,c) at $\rho_{bulk} = 0.10$, 0.25, and 0.50 for each chain length, and in Figure 4 (a,b,c) for $L = 10$, 20, and 40 for each bulk concentration. Note that $\sigma_{total} = \sigma_{sgl} + \sigma_{dbl}$ and $\sigma_{occ} = \sigma_{sgl} + 2\sigma_{dbl}$. The fraction of adsorbed chains that form loops, $\sigma_{dbl}/\sigma_{total}$, is shown in Figure 5. From these figures as well as Figure 6, it is clear that the kinetics of brush formation is complex. In the latter figure the rate of increase in the total

(49) Netz, R. R.; Schick, M. *Macromolecules* **1998**, *31*, 5105.

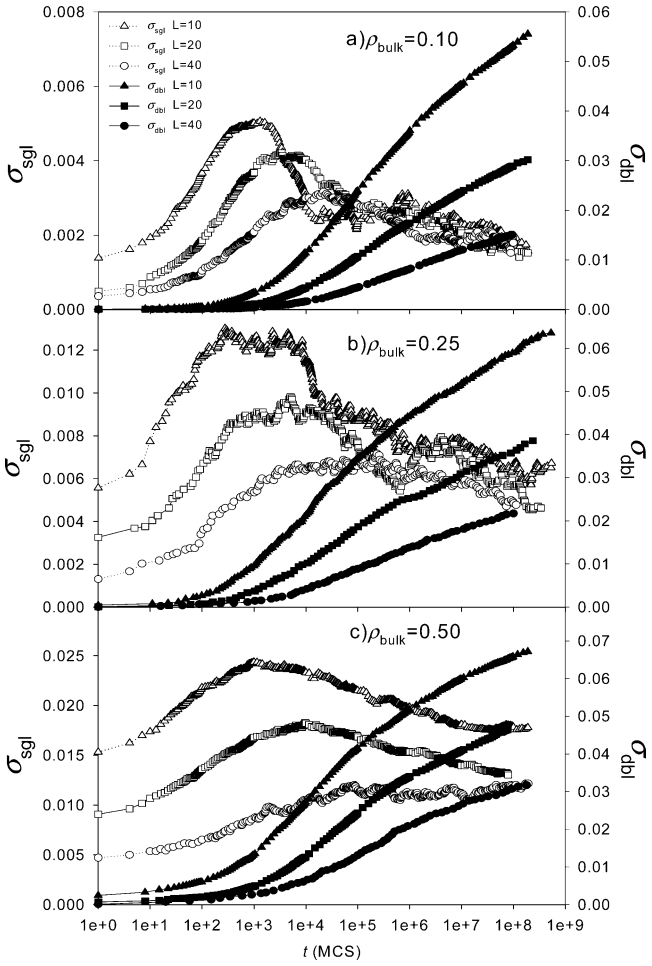

Figure 3. Number of singly bound polymer chains (σ_{sgl}) and the number of doubly bound polymer chains (σ_{dbl}) per unit area as a function of time for $\rho_{bulk} = 0.10$ (a), $\rho_{bulk} = 0.25$ (b), and $\rho_{bulk} = 0.50$ (c) for each chain length studied.

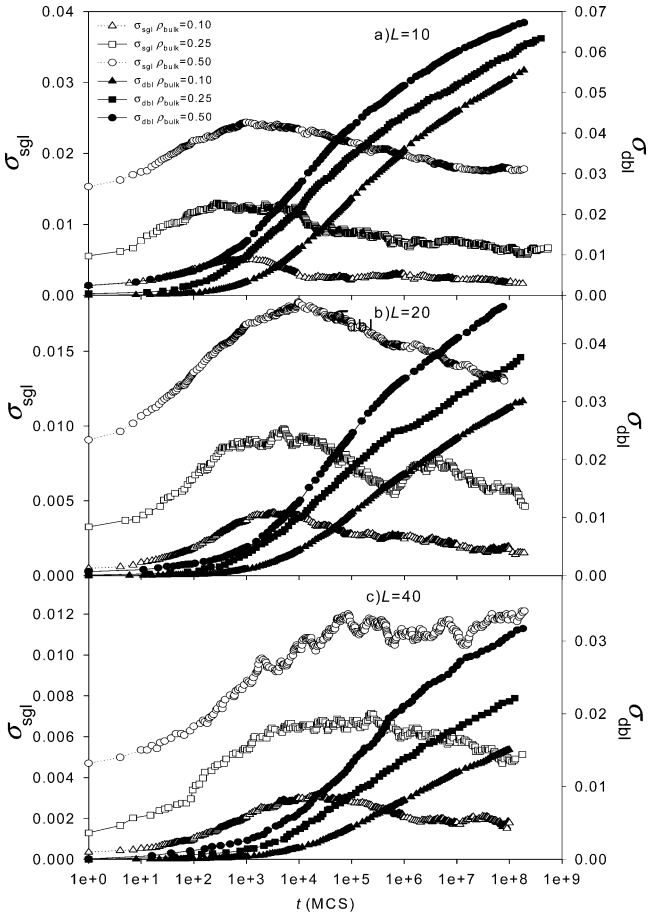

Figure 4. Number of singly bound polymer chains (σ_{sgl}) and the number of doubly bound polymer chains (σ_{dbl}) per unit area as a function of time for $L = 10$ (a), $L = 20$ (b), and $L = 40$ (c) for each bulk density studied.

concentration of adsorbed chains ($d\sigma_{total}/dt$), the rate of formation of loops ($d\sigma_{dbl}/dt$) and the time dependence of σ_{sgl} for $\rho_{bulk} = 0.10$, $L = 10$ are compared. Note that this system exhibits behavior typical of all systems studied. Although $d\sigma_{total}/dt$ decreases monotonically with time, $d\sigma_{dbl}/dt$ exhibits more complex behavior at relatively short times and decreases monotonically only for longer times. σ_{sgl} exhibits a well-pronounced short-time maximum and a second, less pronounced longer-time maximum for most of the systems studied, followed finally by a slow monotonic decrease at long times.

We found that the complex kinetics of brush formation can best be understood by considering various "regimes" of adsorption defined by the primary physics that limits the rate of chain adsorption over the time domain associated with each regime. Here we briefly introduce these regimes as denoted in Figure 6 for the $\rho_{bulk} = 0.10$, $L = 10$ system.

A. Initial Adsorption Regime. The adsorption of chain ends that occurs at $t = 0$ (see Figures 3 and 4) corresponds to adsorption of chain ends that are in contact with the substrate at the time the reaction with the substrate is "turned on". This initial adsorption leads to a low concentration of almost entirely singly bound chains (Figure 5). The number of chains adsorbed at $t = 0$ depends on the equilibrium concentration of end groups at the wall, and hence is proportional to bulk concentration and inversely proportional to chain length. For greater bulk concentrations and short chains there is also a very small quantity of doubly bound chains formed at $t = 0$.

B. Diffusion-Limited Regime. The initial adsorption regime is followed by rapid adsorption of chains as free chain ends not initially in contact with the wall come into contact with the wall. An important characteristic of the diffusion-limited regime (DLR) that follows immediately upon the initial adsorption regime is that the concentration of singly bound chains becomes sufficiently large that loop formation becomes significant and the brush becomes increasingly dominated by loops (Figure 5). The most dominant feature of the DLR is the maximum in σ_{sgl}. In the DLR chain adsorption is limited primarily by diffusion of free chains to the substrate from the bulk solution as discussed in detail in section IV. This regime ends when the brush becomes sufficiently well-formed that the adsorption of chain ends is no longer limited only by diffusion of chains from the bulk solution but becomes increasingly dominated by the need of chains to penetrate through the maturing brush to reach the substrate.

C. Intermediate Regime. The onset of the intermediate regime (IR) (see Figure 6) occurs after the (first) maximum σ_{sgl} and persists until the second maximum in σ_{sgl} observed in many of the systems. During the IR the concentration of singly bound chains at first decreases rapidly and then typically begins to increase slowly. As is found during the DLR, the rate of new chain adsorption decreases monotonically with time in the IR. The rate of loop formation also decreases monotonically with time in the IR. The decreasing rates of new chain adsorption and loop formation with time are largely the result of densification of the brush. Hence the IR is characterized by transition from diffusion-limited chain adsorption, where the rate of chain adsorption is limited primarily by diffusion of chains from the

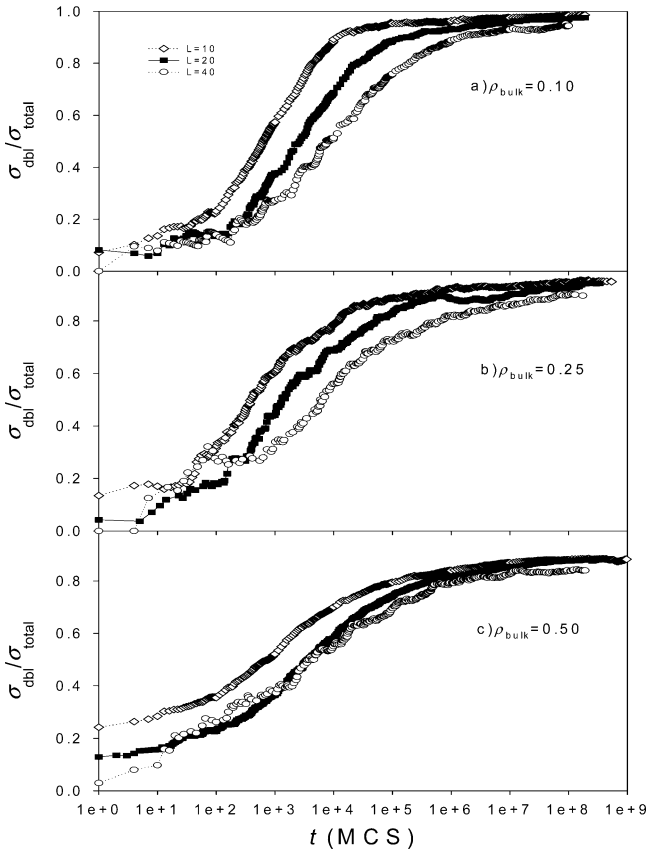

Figure 5. Fraction of adsorbed chains that are doubly bound as a function of time for $\rho_{bulk} = 0.10$ (a), $\rho_{bulk} = 0.25$ (b), and $\rho_{bulk} = 0.50$ (c) for each chain length studied.

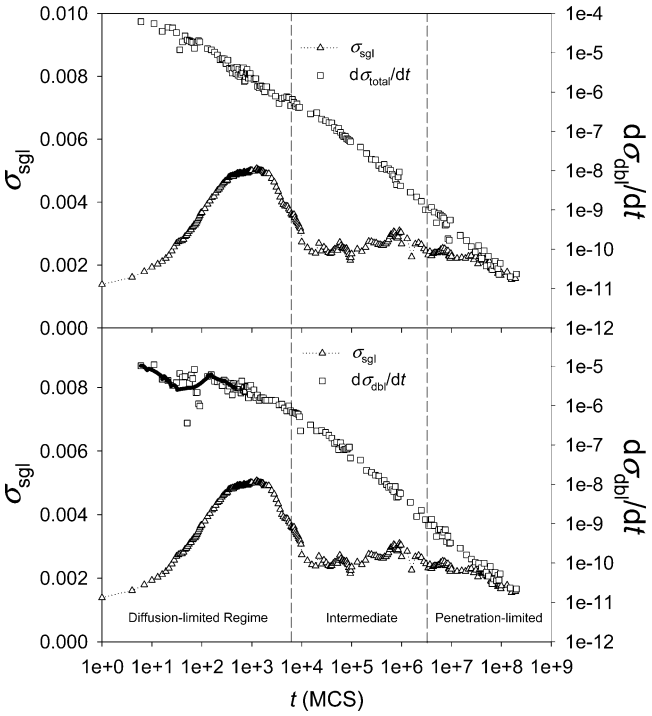

Figure 6. Number of singly bound polymer chains (σ_{sgl}) and the time derivative of the total number of adsorbed chains ($d\sigma_{total}/dt$) (a) and number of double-bound polymer chains ($d\sigma_{dbl}/dt$) (b) for the $\rho_{bulk} = 0.10$, $L = 10$ system. Also shown are the regimes of chain adsorption for this system (see text). The solid line at short times for $d\sigma_{dbl}/dt$ was obtained by smoothing over time.

bulk, to a penetration-limited regime where the brush is now

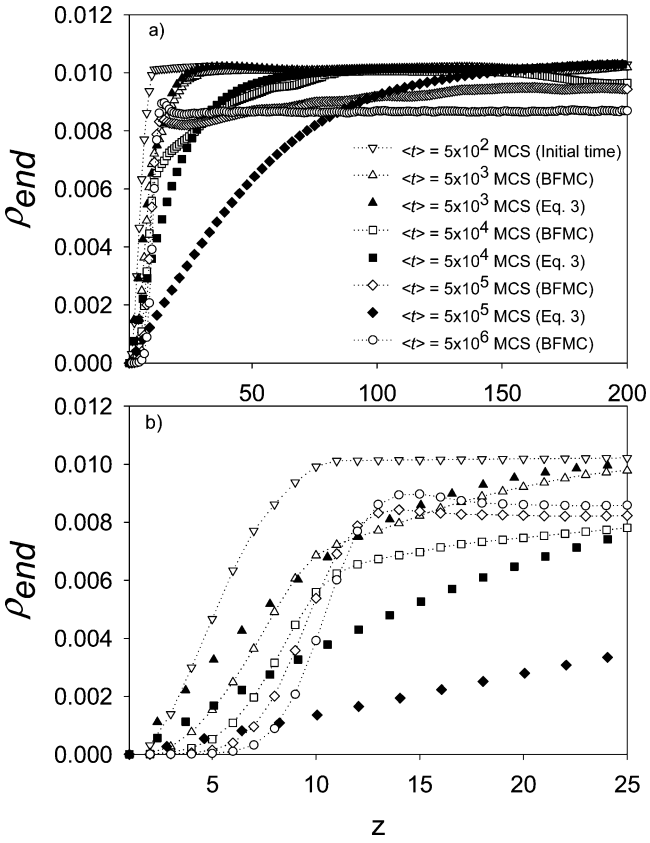

Figure 7. (a) Concentration of end groups of free (unabsorbed) chains for the $\rho_{bulk} = 0.10$, $L = 10$ system as a function of distance from the substrate for various times. The open symbols are from BFMC simulations and the close symbols are from predictions of the diffusion-limited model. (b) Same as (a) near the substrate ($z < 25$).

well-formed and the rate of chain adsorption is limited by penetration of chains through the brush.

D. Penetration-Limited Regime. The penetration-limited regime (PLR) (see Figure 6) is characterized by a slow monotonic decrease in concentration of singly bound chains. In this regime, the rates of new chain adsorption and loop formation continue to decrease monotonically with time due to continual densification of the brush. Brush densification influences the rate of new chain adsorption somewhat more than the rate of double-bound chain formation, accounting for the slowly decreasing concentration of singly bound chains in the PLR. The PLR is discussed in detail in section V.

IV. Analysis of the Diffusion-Limited Regime

Both experiment and simulation studies have indicated that the initial adsorption of monochelic (singly functionalized chains) onto a solid substrate is diffusion limited.[35,50−52] Here we investigate the applicability of a diffusion-limited model to the short-time adsorption observed in our simulations for telechelic chains.

A. Free End Density Profiles for the $\rho_{bulk} = 0.10$, $L = 10$ System. Figure 7 shows the concentration of end groups of free (nonabsorbed) chains for the $\rho_{bulk} = 0.10$, $L = 10$ system as a function distance from the substrate for various adsorption times. Only the end group of each chain that is closest to the substrate

(50) Tassin, J. F.; Siemens, R. L.; Tang, W. T.; Hadziioannou, G.; Swaler, J. D.; Smith, B. A. *J. Chem. Phys.* **1989**, *93*, 2106.
(51) Motschmann, H.; Stamm, M.; Topracioglu, C. *Macromolecules* **1991**, *24*, 6477.
(52) Zajac, R.; Chakrabarti, A. *Phys. Rev. E* **1994**, *49*, 3069.

is considered. Note that when one end of a chain adsorbs to the substrate that chain is no longer free and hence the chain no longer contributes any end group to the free end density profiles. We observe that at short times the concentration of free ends decreases within both the brush (see brush density profile shown in Figure 2 for brush dimensions) and the bulk solution in the neighborhood of the brush while the free end concentration gradient extends further into the bulk solution with time, indicating that the flux of chains to the substrate is dominated by diffusion of the chains through the bulk solution. At longer times the concentration gradient of free ends in the bulk solution largely disappears and the concentration gradient within the brush becomes steeper indicating that flux to the substrate is dominated by transport through the brush.

B. Diffusion-Limited Model for Brush Formation. Under the assumption that the rate of chain adsorption is determined by diffusion of free ends to the substrate, the concentration profile of free ends at time t and distance z from the substrate during the adsorption process is given as the solution to the one-dimensional diffusion equation[53]

$$\frac{\partial c_{\text{free}}(z,t)}{\partial t} = D_{\text{free}} \nabla^2 c_{\text{free}}(z,t) \tag{3}$$

where c_{free} and D_{free} are the concentration and diffusion coefficient for free ends, respectively. Here we assume that the growing brush is not sufficiently mature to significantly influence the chemical potential of free ends, which is consequently determined solely by their concentration. Once D_{free} is established (see below), eq 3 can be integrated numerically as shown in Appendix 1 to yield $\sigma_{\text{total}}(t)$, $\sigma_{\text{dbl}}(t)$, and $\sigma_{\text{sgl}}(t)$.

C. Determination of D_{free}. $\sigma_{\text{total}}(t)$ obtained from BFMC simulations is shown in Figure 8 as a function of adsorption time for all systems studied. For diffusion-limited adsorption a time-independent diffusion coefficient and an initially constant concentration profile will yield $\sigma_{\text{total}}(t)$ proportional to $t^{1/2}$ during the majority of the adsorption process.[53] $\sigma_{\text{total}}(t)$ as shown in Figure 8 increases much more weakly with time than would be indicated by a time-independent diffusion coefficient. We believe this effect is due to contribution of internal chain modes to motion of chain ends on short times scales. Internal modes allow the chain ends to move much faster than the chain center-of-mass over short distances (comparable to the dimensions of the chain) yielding an (apparent) mobility of the chain ends that decreases with time. The apparent diffusion coefficient for chain ends can be determined from the relationship

$$D_{\text{app}}(t) = \frac{\langle r^2(t) \rangle}{6t} \tag{4}$$

where $\langle r^2(t) \rangle$ is the mean-square displacement of chain ends after time t. Simulations were performed on cubic systems with 3-D periodic boundary conditions in order to determine $D_{\text{app}}(t)$. In the limit of long time $D_{\text{app}}(t)$ is equal to the polymer self-diffusion coefficient which depends on concentration and chain length and is determined from the mean-square displacement of the center-of-mass of the polymer chains.

In our modeling of the DLR, we assume that the rate at which chain ends diffuse to the substrate is related to $D_{\text{app}}(t)$ obtained from bulk solution simulations. We therefore allow the free end

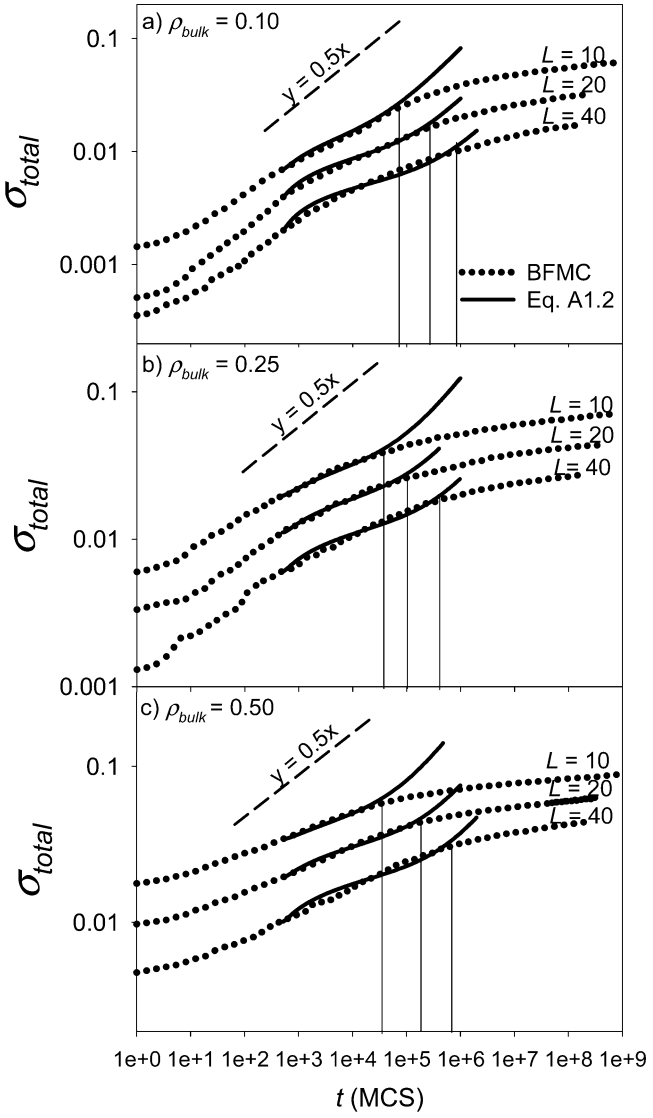

Figure 8. $\sigma_{\text{total}}(t)$ as a function of time for $\rho_{\text{bulk}} = 0.10$ (a), $\rho_{\text{bulk}} = 0.25$ (b), and $\rho_{\text{bulk}} = 0.50$ (c) for each chain length studied. Dotted lines are from BFMC simulations. The dashed line indicates a slope of 1/2. The solid lines are obtained from numerical integration of eq A1.2 using the best-fit end-group diffusion coefficients given in Table 2. The solid vertical lines indicate the end of the diffusion-limited regime for each system.

diffusion coefficient to be a decreasing function of time with a form

$$D_{\text{free}}(t) = D_0 + \frac{D_1}{t} \tag{5}$$

where D_0 is the polymer self -diffusion coefficient obtained from bulk solution simulations. The value of D_1 was adjusted to obtain the best representation of $\sigma_{\text{total}}(t)$ (eq A1.2) in the vicinity of t_{initial}. Values of D_0 and D_1 are given in Table 2. A value of $t_{\text{initial}} = 500$ MCS was utilized for all systems (see Table 2). For most systems similar values of D_1 were obtained when t_{initial} was reduced to 100 MCS. The ratio of $D_{\text{free}}(t)$ (from fits) to $D_{\text{app}}(t)$ from bulk solution simulations is shown for the $\rho_{\text{bulk}} = 0.10$ systems in Figure 9. Agreement is reasonable and deviations between $D_{\text{free}}(t)$ and $D_{\text{app}}(t)$ at very short times can be understood in terms of the perturbation of the chain conformations by the substrate. When reaction with the wall is turned on ($t = 0$) the conformations of chains with their center-of-mass near the substrates have been

(53) Crank, J. *The mathematics of diffusion*, 2nd ed.; Clarendon Press: Oxford, U.K., 1975.

Table 2. Properties of the Diffusion-Limited Regime

				DLR→IR[b]			
ρ_{bulk}	L	D_0, D_1 (l^2/MCS, l^2)	$t_{initial}$[a] (MCS)	log $\tau_{DLR\rightarrow IR}$ (MCS)	σ_{occ} (l^{-2})	σ_{occ}/R_e (l^{-3})	k_{dbl}
0.10	10	3.0×10^{-3}, 18.0	500	4.9	0.048	0.47	$0.14D_{free}$
	20	1.3×10^{-3}, 27.0	500	5.3	0.030	0.45	$0.053D_{free}$
	40	7.0×10^{-4}, 37.0	500	6.0	0.018	0.41	$0.022D_{free}$
0.25	10	9.0×10^{-4}, 9.0	500	4.6	0.068	0.65	$0.16D_{free}$
	20	7.8×10^{-4}, 15.5	500	5.0	0.045	0.64	$0.060D_{free}$
	40	5.0×10^{-4}, 23.0	500	5.7	0.032	0.67	$0.034D_{free}$
0.50	10	6.4×10^{-4}, 5.0	500	4.6	0.095	0.84	$0.16D_{free}$
	20	2.8×10^{-3}, 8.5	500	5.2	0.070	0.92	$0.087D_{free}$
	40	2.2×10^{-3}, 13.5	500	5.9	0.052	0.99	$0.043D_{free}$

[a] Initial time used in modeling the diffusion-limited regime. [b] Onset time for the intermediate regime and associated properties.

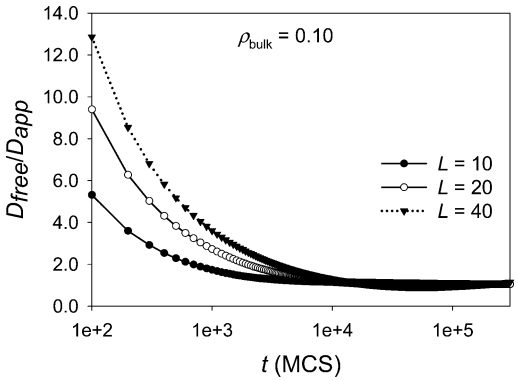

Figure 9. Comparison of $D_{free}(t)$ and $D_{app}(t)$ for $\rho_{bulk} = 0.10$ for the three chain lengths studied.

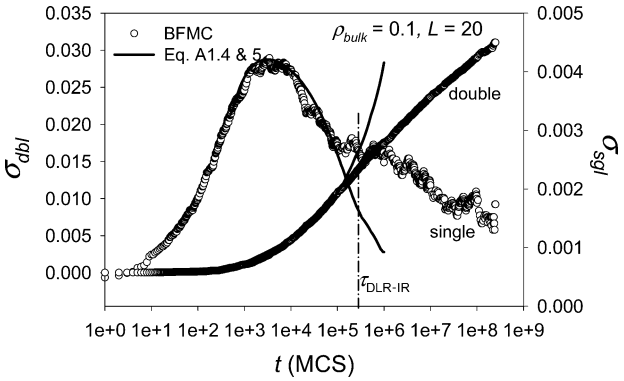

Figure 10. $\sigma_{sgl}(t)$ and $\sigma_{dbl}(t)$ for the $\rho_{bulk} = 0.10$, $L = 20$ system as predicted by the diffusion-limited model and obtained from BFMC simulations. The vertical line shows $\tau_{DLR\rightarrow IR}$.

perturbed by the substrate, with end-groups preferentially near the substrate. At later times adsorption involves chains approaching the substrate from the bulk solution that have not had an opportunity to fully equilibrate to the presence of the substrate before reacting and the end-groups of these chains exhibit dynamics more similar to those of the unperturbed bulk solution chains given by $D_{app}(t)$.

D. Predictions of $\sigma_{total}(t)$, $\sigma_{sgl}(t)$, and $\sigma_{dbl}(t)$ in the Diffusion-Limited Regime. We assign the time at which significant deviation occurs between $\sigma_{total}(t)$ predicted by the diffusion-limited model (eq A1.2) with that obtained from BFMC simulations (see Figure 8) as the limit of the DLR and the onset of the IR. These times ($\tau_{DLR\rightarrow IR}$) are given in Table 2. Once the IR is entered, the diffusion-limited model overestimates $\sigma_{total}(t)$ indicating that the growing brush reduces the rate of chain adsorption compared to that predicted by the diffusion-limited adsorption model.

The diffusion-limited model also provides predictions for $\sigma_{sgl}(t)$ and $\sigma_{dbl}(t)$ (eqs A1.4 and A1.5) once the reaction rate constant k_{dbl} is determined. We have found that the representation of $\sigma_{sgl}(t)$ and $\sigma_{dbl}(t)$ obtainable by assuming k_{dbl} to be constant with time to be unsatisfactory. A much better representation can be obtained by allowing k_{dbl} to decrease with time. Physically this is a consequence of the fact that the conformations of chains near the solid substrates when "reaction" between the chain ends and the substrate is turned on (following equilibration) are perturbed by the presence of the substrate. These chains, which are the first to adsorb, tend to have their second end nearer the substrate when adsorption of the first end occurs than chains that must move larger distances to reach the substrate and hence are relatively unperturbed by the substrate when their first end is adsorbed. The nearer the second end is to the substrate when the first end adsorbs, the faster the chain (on average) converts from a singly bound chain to a loop, and hence the greater k_{dbl}.

In practice we have found that a reasonable representation of $\sigma_{sgl}(t)$ and $\sigma_{dbl}(t)$ in the diffusion-limited regime can be obtained by allowing k_{dbl} to be proportional to D_{free}. The resulting proportionality constants are given in Table 2. A comparison of the predicted $\sigma_{sgl}(t)$ and $\sigma_{dbl}(t)$ (eqs A1.4 and A1.5) and results from BFMC simulation is shown in Figure 10 for a representative system. Once the IR has been entered (i.e., predictions of the total adsorption exceed the actual adsorption), the diffusion-limited model dramatically overestimates $\sigma_{dbl}(t)$ and underestimates $\sigma_{sgl}(t)$, indicating that the influence of the growing brush in the IR on the rate of formation of loops is even greater than its influence on the rate of adsorption of new chains.

E. Concentration Profiles for the $\rho_{bulk} = 0.10$, $L = 10$ System. Employing the profile $c_{free}(z,t_{initial} = 500)$ obtained from BFMC simulations for initial conditions for the $\rho_{bulk} = 0.10$, $L = 10$, the profile $c_{free}(z,t)$ at various times has been predicted by numerical solution of eq 3. A comparison with the actual profiles obtained from BFMC simulation is shown in Figure 7. Reasonable agreement is seen at short times, (e.g., $\langle t \rangle = 5 \times 10^3$) with deviation increasing with increasing adsorption time. For times greater than $\tau_{DLR\rightarrow IR}$ (7.8×10^4 MCS, Table 2), the profiles begin to differ qualitatively. Here, the diffusion-limited model predicts continuing extension of the free end density gradient into the bulk solution. In contrast, the BFMC simulations reveal that the bulk gradient begins to disappear once the IR is entered. Furthermore, quantitative deviations between the predicted $c_{free}(z,t)$ and BFMC simulation results are apparent at times shorter than $\tau_{DLR\rightarrow IR}$ (Figure 7b). Hence, even at short times the nascent brush influences free end concentration gradients and transport within the brush. The relatively weak free end gradient for $z <$ 5−6 is likely the result of fast approach to the surface for chain ends that have penetrated inside the first "blob" of the adsorbed polymer chains,[39] whereas the steepening free end gradient within the brush for $z > 6$ with time reflects increasing steric hindrance

Table 3. Properties of the Penetration-Limited Regime

		IR→PLR[a]							
ρ_{bulk}	L	log $\tau_{IR\rightarrow PLR}$ (MCS)	σ_{occ} (l^{-2})	σ_{occ}/R_e (l^{-3})	log t_{min}, t_{max}[b] (MCS, MCS)	β_{dbl}[c]	β_{dbl}/R_g^2	β_{sgl}[d]	β_{sgl}/R_g^2
0.10	10	5.8	0.07	0.69	6.0, 8.4	14.5	0.88	15.7	0.95
	20	6.1	0.04	0.62	6.0, 8.4	30.8	0.80	33.6	0.87
	40	was not fit							
0.25	10	6.8	0.11	1.04	7.0, 8.0	13.1	0.86	14.0	0.92
	20	6.7	0.06	0.86	6.7, 8.0	28.3	0.82	30.3	0.88
	40	was not fit							
0.50	10	7.8	0.15	1.32	8.0, 8.3	12.9	0.96	13.1	0.97
	20	7.8	0.10	1.31	7.8, 8.1	19.5	0.67	20.0	0.68
	40	was not fit							

[a] Onset time for the penetration-limited regime and the corresponding properties. [b] Range of data used in determining the surface occupancy scaling behavior of the rate constants (eqs 10−11). [c] Equation 11. [d] Equation 10.

for free chains transport to the substrate with growth of the brush. To more accurately predict $c_{free}(z,t)$ in the DLR, it would be necessary to account for the influence of the growing brush on free end penetration, e.g., by allowing D_{free} to depend on position relative to the substrate.

V. Kinetic Analysis of the Penetration-Limited Regime

Simulations, experiment and theoretical studies of the adsorption of monochelic chains to solid substrates reveal that after sufficient adsorption has occurred further adsorption no longer follows the $t^{1/2}$ scaling behavior predicted by the ideal diffusion-limited model.[39,53] This behavior has been associated with steric effects of the growing brush slowing adsorption (kinetic barrier),[39] and increased stretching of the chains with brush growth (thermodynamic barrier).[54] We have analyzed the adsorption kinetics in the PLR (introduced in section II.D) based upon the reactions given in eq 2. The net rate of change in the concentration of singly bound chains, the rate of formation of loops and the rate equation for surface occupancy, where $\sigma_{occ}(t) = \sigma_{sgl}(t) + 2\sigma_{dbl}(t)$, are

$$\frac{d\sigma_{sgl}}{dt} = k_{sgl}c_{free}[\sigma_{max}f_A] - k_{dbl}\sigma_{sgl}[\sigma_{max}f_A] = k'_{sgl}[\sigma_{max}f_A] - k_{dbl}\sigma_{sgl}[\sigma_{max}f_A] \quad (6)$$

$$\frac{d\sigma_{dbl}}{dt} = k_{dbl}\sigma_{sgl}[\sigma_{max}f_A] \quad (7)$$

$$\frac{d\sigma_{occ}}{dt} = k'_{sgl}[\sigma_{max}f_A] + k_{dbl}\sigma_{sgl}[\sigma_{max}f_A] \quad (8)$$

where

$$f_A(t) = (\sigma_{max} - \sigma_{occ}(t))/\sigma_{max} \quad (9)$$

is the fraction of surface sites still accessible after time t. In the PLR, we assume that brush formation is limited by penetration of the brush by free chains and not by diffusion of free chains to the brush; hence, c_{free}, the concentration of free ends in contact with the brush, is constant (see for example Figure 7 for longer times). Our approach in analyzing the PLR is to estimate the unknown rate constants $k'_{sgl}(f_A)$ and $k_{dbl}(f_A)$ from BFMC data as described in detail in Appendix 2. The rate constants were then fit with a power law in $f_A(t)$

$$k'_{sgl}(f_A) = \alpha_{sgl}f_A^{\beta_{sgl}-1}/\sigma_{max} \quad (10)$$

$$k_{dbl}(f_A) = \alpha_{dbl}f_A^{\beta_{dbl}-1}/\sigma_{max} \quad (11)$$

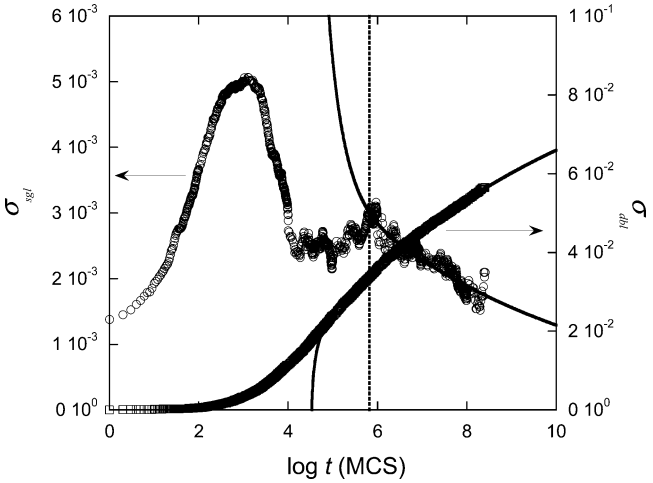

Figure 11. $\sigma_{sgl}(t)$ and $\sigma_{dbl}(t)$ for the $\rho_{bulk} = 0.10$, $L = 10$ system as predicted by the penetration-limited model and obtained from BFMC simulations. The vertical line shows $\tau_{IR\rightarrow PLR}$.

The resulting scaling exponents are given in Table 3 and are discussed in section VI.C.

Starting at times corresponding to the beginning of the fitting range (see Table 3), eqs 6−8 were numerically integrated forward and backward in time utilizing the power-law expressions for the rate constants to determine $\sigma_{sgl}(t)$, $\sigma_{dbl}(t)$, and $f_A(t)$. A comparison of the model predictions for $\sigma_{sgl}(t)$ and $\sigma_{dbl}(t)$ with BFMC simulation results for the $\rho_{bulk} = 0.10$, $L = 10$ system is shown in Figure 11. The onset of the PLR, $\tau_{IR\rightarrow PLR}$, is shown. For times shorter than $\tau_{IR\rightarrow PLR}$, $\sigma_{sgl}(t)$ no longer increases monotonically with decreasing time and the penetration-limited model is not applicable. $\tau_{IR\rightarrow PLR}$ and the corresponding surface occupancy for all systems for which it was possible to model the brush kinetics in the PLR are given in Table 3. Our inability to model the PLR for several systems is discussed in section VI.C. Good agreement for $\sigma_{sgl}(t)$ and $\sigma_{dbl}(t)$ between the penetration-limited model and BFMC simulations can be seen in the PLR. For times corresponding to the IR the model overestimates $\sigma_{sgl}(t)$ and $\sigma_{total}(t)$ indicating that the scaling behavior of rate constants that holds in the PLR does not hold in the IR, revealing that additional effects that slow the rate of brush growth in the IR compared to that predicted by the PLR model are operative. For example, Figure 7 reveals that during the IR there still exists a gradient in the concentration of free chains in the bulk solution that disappears only when the PLR is entered, resulting in a lower c_{free} at the brush surface in the IR than is found in the PRL.

Figure 12 shows the predicted behavior of $\sigma_{sgl}(t)$, $\sigma_{dbl}(t)$, and $f_A(t)$ extended to very long time for the $\rho_{bulk} = 0.10$, $L = 10$

(54) O'Shaughnessy, B.; Sawhney, U. *Phys. Rev. Lett.* **1996**, *76*, 3444.

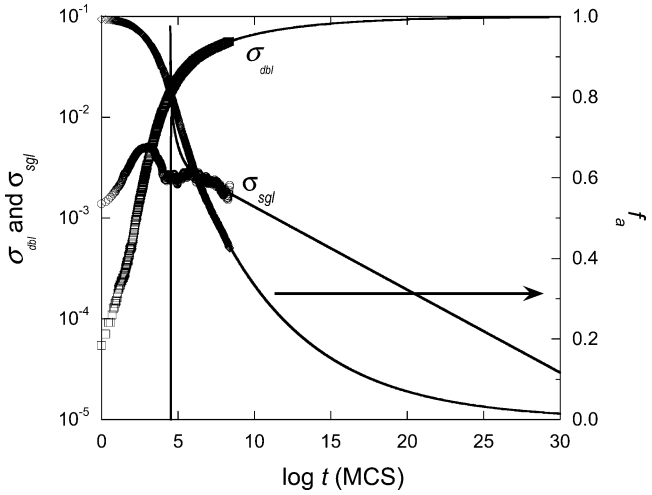

Figure 12. $\sigma_{sgl}(t)$, $\sigma_{dbl}(t)$, and $f_A(t)$ for the $\rho_{bulk} = 0.10$, $L = 10$ system as predicted by the penetration-limited model for long times.

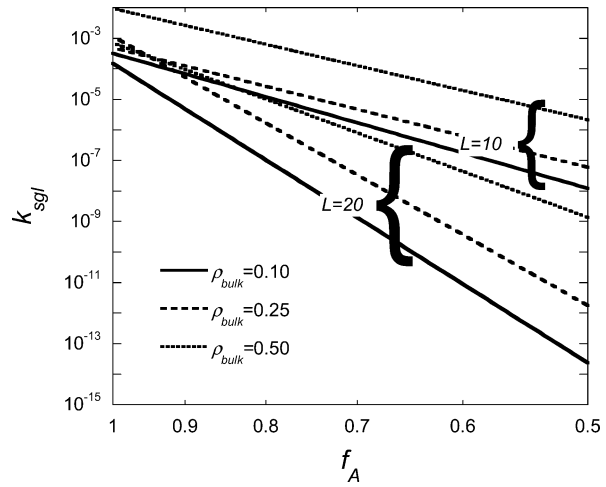

Figure 13. Rate constant k_{sgl} obtained from BFMC simulations as a function of surface occupancy.

system. At the onset of the PLR, the substrate is only partially occupied (see Table 3) and the brush continues to grow slowly during the PLR. The concentration of singly bound chains decreases monotonically, reaching zero only when substrate is completely occupied, i.e., the brush is fully formed ($f_A = 0$). We find that the brush is increasingly dominated by loops in the PLR (see also Figure 5). Figure 12 reveals that the growth process in the PLR is slow and decreases dramatically with time, consistent with the strong scaling of the rate constants with surface coverage. The rate constant for adsorption of new chains, k_{sgl} is shown in Figure 13 as a function of f_A. The dramatic decrease in the rate constants (k_{dbl} exhibits analogous behavior) with f_A is apparent. Clearly, it becomes increasingly difficult either for new chains to penetrate the brush or for loops to form from singly bound chains as the brush matures. The chain length and solution concentration dependence of the rate constants, scaling exponents, and onset time for the PLR are discussed in section VI.C.

Finally, we note that although σ_{total} does not follow $t^{1/2}$ behavior in the PLR, as expected, neither does the amount of adsorbed material follow exponential time behavior as reported in previous simulation, experimental and theoretical studies.[35,39] This can be seen in Figures 12 and 13 (note that $\sigma_{total} \approx \sigma_{dbl}$ in the PLR) for both the time domain covered by our BFMC simulations and the extrapolated time domain utilizing the model described above. This discrepancy may be due to the much longer domain of time (relative to the onset of the PLR) covered by our simulations compared to previous simulations. We find that over a sufficiently short time domain the time dependence of σ_{total} can be reasonably described as exponential (or alternatively, power-law) whereas over longer time domains the time dependence of σ_{total} cannot be described by a simple scaling relationship. We also note that previous simulations[35] utilized many fewer chains per unit surface area for the same bulk solution concentration than we have employed; i.e., these systems were much smaller in the *z* direction than those employed in our simulation, with the result that adsorption kinetics in the older studies are influenced by the depletion of chains from the bulk solution and do not reflect kinetics associated with a constant bulk concentration.

VI. Concentration and Chain Length Dependence of Adsorption Kinetics

It is clear from examination of Figures 3 and 4 that the kinetics of brush formation depend on the concentration of polymer in bulk solution and the polymer chain length. Figure 5 reveals that important structural quantities, such as the fraction of attached chains that are doubly bound after a given adsorption time, also depend on bulk solution concentration and chain length. Here we consider in detail the dependence of the kinetic regimes and rates of adsorption and loop formation on bulk solution concentration and chain length.

A. Critical Surface Coverage. Tables 2 and 3 show the surface coverage σ_{occ} associated with the onset of the IR and PLR, respectively. The critical surface coverage for both "transitions" (DLR → IR, IR → PLR) increases with concentration and decreases with chain length. It has been predicted theoretically that the transition from diffusion-limited to penetration-limited behavior for reaction of end-functionalized polymers at an interface should occur at a surface coverage inversely proportional to the size of the polymer chain, i.e., $\sigma_{occ} \propto R_e^{-1}$.[54] Table 3 reveals that the surface coverages associated with the DLR → IR and IR → PLR transitions are reasonably well described by this scaling. If this scaling behavior holds for long chains we can anticipate that both the DLR and IR will eventually vanish; that is, for sufficiently long chains, adsorption will be dominated by penetration of the brush at all times.

The fact that these "critical" surface coverages follow the theoretical predicted scaling behavior is surprising. The theoretical predictions are based upon thermodynamic arguments,[54] where rate constants are dominated by the stretching energy of chains penetrating highly stretched brushes and where the brush height is much greater than R_e and depends on surface coverage. Our brushes do not fall into this classification. As discussed in section II.D, our brush profiles (and heights) in the PLR are consistent with moderately stretched chains and the brush height does not change dramatically with increasing surface coverage for the range of coverage accessible by simulations. Furthermore, equilibrium simulations, performed by allowing brush formation to occur for various periods of time $\tau_{formation}$ followed by equilibration of the system to the (now) static brushes by carrying out additional simulation without further reaction, reveal that the concentration profiles for free ends are largely independent of $\tau_{formation}$ once the IR is entered, i.e., $\tau_{formation} > \tau_{DLR \rightarrow IR}$. Furthermore, the equilibrium free end profiles are quite similar to the dynamic profiles observed during brush growth (e.g., Figure 7) for $\tau_{formation} > \tau_{IR \rightarrow PLR}$; that is, the profiles are characterized by a steep gradient in the concentration of free end from the brush surface to the substrate with a very low concentration of free ends at the interface. These observations lead us to conclude that the change in adsorption kinetics with surface coverage observed in our simulations is primarily a kinetic phenomena

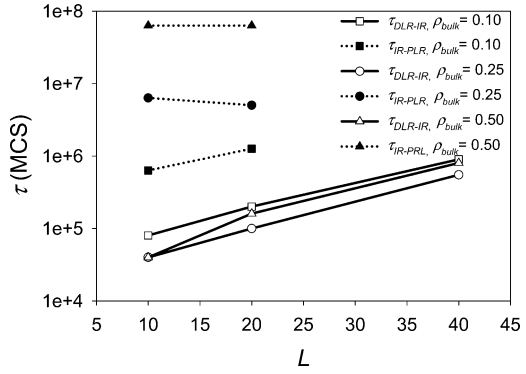

Figure 14. $\tau_{DLR\rightarrow IR}$ and $\tau_{IR\rightarrow PLR}$ for $\rho_{bulk} = 0.10$ (a), $\rho_{bulk} = 0.25$ (b), and $\rho_{bulk} = 0.50$ (c) as a function of chain length.

that can be associated with increasing steric hindrance to penetration of chains provided by the growing brush, and is not primarily due to thermodynamic barriers to penetration associated with chain stretching that increases with surface coverage. Note that the latter effect would become more important for very high coverages/highly stretched chains, and the observed scaling of reaction rates with surface coverage (eqs 10 and 11) may not apply in this highly stretched regime, which in any event is not accessible to simulation or experiment[49] due to slow adsorption kinetics.

We have also looked for correlations between the DLR → IR and IR → PLR transitions and the onset of chain overlap given by $\sigma_{occ} = 1/R_g^2$, tabulated in Table 1. Table 1 reveals that the onset of chain overlap lies near the DLR → IR transition or well within the DLR, depending on chain length and concentration, indicating that no clear correlation between the overlap coverage and the DLR → IR or IR → PLR transitions exists.

B. Regime Transition Times. Figure 14 shows $\tau_{DLR\rightarrow IR}$ and $\tau_{IR\rightarrow PLR}$ as a function of chain length for the various solution concentrations. $\tau_{DLR\rightarrow IR}$ exhibits only weak dependence on concentration but increases strongly with chain length. In contrast, the critical surface occupancy at the onset of the IR decreases with increasing chain length as discussed above, indicating that longer chains are more effective at shielding the substrate from adsorption of free chain ends than shorter chains. Furthermore, for a given bulk chain concentration, the concentration of free chain ends, and hence the driving force for transport of chain ends to the substrate, decreases with increasing chain length. Combined, these effects lead to a transition from the DLR to the IR at lower surface coverage for longer chains. The reduced driving force and reduced diffusion coefficient for longer chains account for the increase in $\tau_{DLR\rightarrow IR}$ with increasing chain length despite the decrease in surface occupancy at $\tau_{DLR\rightarrow IR}$.

In contrast to $\tau_{DLR\rightarrow IR}$, the onset of the PLR, $\tau_{IR\rightarrow PLR}$, exhibits little dependence on chain length but increases dramatically with increasing concentration. During the IR not only is the brush maturing but concentration gradients that have developed in the bulk solution during the diffusion-limited regime are also disappearing. The onset of the PLR corresponds to the disappearance of gradients of free chains in the bulk solution. We speculate that at higher polymer concentrations the bulk concentration gradients that form during the diffusion-limited regime take longer to disappear due to a reduction in diffusion coefficient with increasing concentration, hence extending the IR regime to longer times.

Based upon the trends discussed above, we anticipate that the IR will decrease in duration with increasing chain length as the DLR extends to longer times. With decreasing polymer concentration, we anticipate that the onset of the PLR will continue

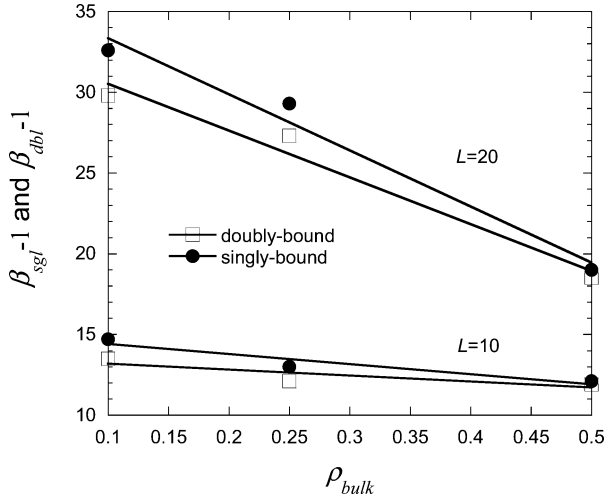

Figure 15. β_{sgl} and β_{dbl} as a function of ρ_{bulk}.

to move to shorter times. Hence, for long chains and low concentration, we expect a direct transition for diffusion-limited to penetration-limited behavior. We also anticipate that the decrease in concentration of singly bonded chains that occurs at the end of the DLR and the beginning of the IR (see Figures 3 and 10) will continue to become less dramatic with increasing chain length and as a consequence the maximum in σ_{sgl} will diminish and eventually vanish, consistent with the trends observable in Figure 3.

C. Influence on Rate Constants in the Penetration-Limited Regime. The rate constants for adsorption of new chains (eq 10) and formation of loops (eq 11) are well-described by power-laws in fraction of available sites f_A. The scaling exponents β_{sgl} and β_{dbl} (Table 3) for adsorption of new chains and formation of loops are shown as a function of ρ_{bulk} in Figure 15 for the systems where clear determination of the PLR was possible. For the longest chains studied ($L = 40$) the statistics were poorest and we were not able to resolve the IR and PLR. From Figure 15, it can be seen that β_{sgl} and β_{dbl} increase dramatically with increasing chain length and decrease somewhat less dramatically with increasing bulk solution concentration of polymer. As a result, for a given surface coverage the rate constants, and the hence rate of brush growth in the PLR, decreases dramatically with increasing chain length and increases less dramatically with increasing bulk concentration, as illustrated in Figure 13. The decrease in rate of adsorption with increasing chain length can be understood in terms of the influence of chain length on the amount of adsorbed material and brush height for a given surface occupancy. For the same number of chains adsorbed, longer chains yield a denser and higher brush thereby providing increased steric resistance to penetration of chain ends to the substrate. The concentration dependence can be understood in terms of the free energy penalty for penetration of the brush by a chain end belonging either to a free chain or a singly attached chain. The density difference in total material (monomers) between the brush (including both adsorbed and nonadsorbed material within the brush) and the bulk solution for a given surface occupancy (f_A) becomes smaller the higher the bulk solution concentration.

The drastic decrease of adsorption rate with increasing chain length and surface coverage are qualitatively consistent with previous BFMC studies of single-chain adsorption through a preformed monochelic brush.[39] Additionally, we find that β_{sgl} and β_{dbl} scale reasonably well with R_g^2, particularly for $\rho_{bulk} = 0.10$ and 0.20, as shown in Table 3. This behavior results in a scaling variable of $\sigma_{occ}R_g^2$ for the rate of adsorption suggested in the earlier study of preformed monochelic brushes for $\sigma_{occ} \ll$

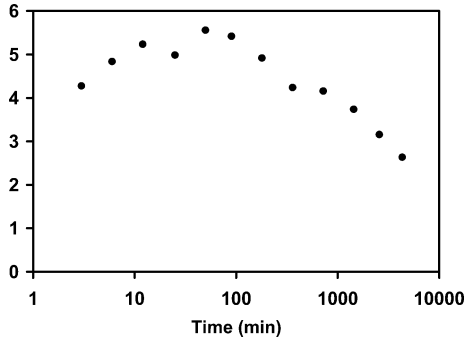

Figure 16. Plot of fluorescence from fluorescently tagged bound telechelics as a function of reaction time between telechelics and a functionalized surface. The fluorescence is proportional to the amount of singly bound chains and compares favorably to the simulation results of Figure 3.

σ_{max} (see Appendix 3). However, $\sigma_{occ}R_g^2$ is not an applicable scaling variable for the surface occupancies corresponding to the PLR for the finite concentrations studied in this work, which do not fulfill the $\sigma_{occ} \ll \sigma_{max}$ criterion.

VII. Correlation to Experimental Formation of Doubly-Bound Polymers Brushes

A. Preliminary Experimental Results. The time evolution of singly bound chains in the reaction of telechelics to a functionalized substrate has been determined experimentally. Here, a silicon wafer was functionalized with epoxy groups by self-assembly techniques. Onto this epoxy-covered surface, a thin film of dicarboxylic acid polystyrene telechelics ($M_n = 3500$) is spin-coated. This system is annealed at 150 °C in a vacuum for various reaction times to allow the reaction of the carboxylic acid to the epoxy surface to bind the polystyrene to the surface. The sample is then washed and sonicated for 20 h to remove all unbound polymer. Ellipsometry and contact angle experiments verify the presence of bound polystyrene, presumably consisting of singly bound and doubly bound chains on the surface. The amount of dangling carboxylic acid groups (and thus singly bound polystyrene chains) is then monitored by fluorescent tagging. This layer is reacted for 24 h with l-pyrenyldiazomethane (PDAM), a robust fluorescent molecule that readily reacts with carboxylic acids at room temperature without catalyst.[55] The fluorescence of the resultant surface is then monitored and the results are shown in Figure 16. In this experiment, the fluorescence corresponds to the amount of singly bound chains present.

B. Comparison of BFMC Predictions and Experiment. Comparison of Figures 16 and 3 reveals excellent correlation between experimental and simulation results, where both systems exhibit an increase in amount of singly bound with early times, a maximum, and further decrease at later times as the singly bound chains form loops. This qualitative agreement is important for several reasons. First, it provides direct validation of model predictions, where complex behavior first predicted by the BFMC simulations was later confirmed by experiments. This validation indicates that much of the fundamental physics controlling the kinetics of brush formation by irreversible adsorption of telechelic polymers onto a solid substrate is captured by the BFMC model. For example, this agreement supports our assumption of first-order reaction kinetics (eq 2) between the telechelic polymers and the substrate: strongly correlated reactions due to clustering of functional chain ends in solution or on the surface would yield qualitatively different brush formation kinetics. Second, attempts to quantitatively assign a time scale to the BFMC model by correlating the point of maximum $\sigma_{sgl}(t)$ from BFMC simulations and experiment have revealed that experimentally the maximum occurs at a much later time than predicted by the BFMC simulations, indicating that for the particular experimental system investigated the reaction rate of telechelic chain ends with the functionalized surface is much slower than the rate of diffusion of chain ends to the surface. We are currently extending the BFMC simulations to include the effects of finite reaction rates between chain ends and the substrate and will present a detailed quantitative comparison of predictions of the extended model with experiment in a future paper.

(55) Nimura, N.; Kinoshita, T.; Yoshida, T.; Uetake, A.; Nakai, C. *Anal. Chem.* **1988**, *60*, 2067.

VIII. Conclusions

We have conducted extensive simulations studies of the kinetics of brush formation by irreversible adsorption of telechelic polymers from solution and melts onto a solid substrate utilizing the BFMC model. The BFMC model predicts complex kinetics that are found to be qualitatively in agreement with experiment. We anticipate that extensions of the BFMC model, in particular inclusion of a finite reaction between chain ends and the substrate will allow us to quantitatively reproduce experimentally observed kinetics of brush formation. Analysis of the kinetics of brush formation obtained from BFMC simulations utilizing simple diffusion-limited and penetration-limited analytically models for the short-time and long-time behavior, respectively, have provided important insight into the mechanism of brush formation, particularly the formation of loops, and provide useful tools for predicting brush structure and kinetics on time scales well beyond those directly accessible to the BFMC simulations.

Acknowledgment. The authors gratefully acknowledge support of the National Science Foundation through a Collaborative Research in Chemistry Grant (CHE-0304807).

X. Appendices

Appendix 1. Beginning with eq 3, flux of chains to the substrate as a function of time is given by

$$\frac{\partial \sigma_{total}(t)}{\partial t} = -D_{free}\frac{\partial c_{free}(z,t)}{\partial z}\Big|_{substrate} \qquad (A1.1)$$

Initial conditions are established by the profile $c_{free}(z,t_{initial})$ obtained from BFMC simulations at some short time $t_{initial}$. Boundary conditions are $c_{free}(0,t) = 0$ (substrate) and $\partial c_{free}(z_{center},t)/\partial t = 0$ (zero flux at the center of the simulation cell). Time integration yields

$$\sigma_{total}(t) = \sigma_{total}(t_{initial}) - \int_{t_{initial}}^{t} D_{free}\frac{\partial c_{free}(z,t)}{\partial z}\Big|_{substrate} dt \qquad (A1.2)$$

When eqs A1.2 and 2 are combined, the rate of formation of singly bound chains is given by

$$\frac{\partial \sigma_{sgl}(t)}{\partial t} = -D_{free}\frac{\partial c_{free}(z,t)}{\partial z}_{surface} - k_{dbl}\sigma_{sgl}(t)\sigma_A(t) \qquad (A1.3)$$

where $\sigma_A(t)$ is the surface concentration of unoccupied (i.e., available) binding sites, $\sigma_A(t) = \sigma_{max} - \sigma_{occ}(t)$. Integrating this

equation, we obtain

$$\sigma_{sgl}(t) = \sigma_{sgl}(t_{initial}) - \int_{t_{initial}}^{t} D_{free} \frac{\partial c_{free}(z,t)}{\partial z}_{surface} dt - \int_{t_{initial}}^{t} k_{dbl}\sigma_{sgl}(t)\sigma_A(t)\, dt \quad (A1.4)$$

$$\sigma_{dbl}(t) = \sigma_{dbl}(t_{initial}) + \int_{t_{initial}}^{t} k_{dbl}\sigma_{sgl}(t)\sigma_A(t)\, dt \quad (A1.5)$$

Appendix 2. Equations 6 and 7 can be rearranged yielding

$$k_{dbl}(f_A)f_A\sigma_{max} = \frac{d\sigma_{dbl}}{dt}/\sigma_{sgl} \quad (A2.1)$$

$$k'_{sgl}(f_A)f_A\sigma_{max} = \frac{d\sigma_{sgl}}{dt} + \frac{d\sigma_{dbl}}{dt} \quad (A2.2)$$

We assume that the rate constants decrease monotonically in the PLR with increasing surface occupation in a well-behaved manner. A consequence of this assumption is that the brush growth kinetics can be described using this approach only for times beyond which $\sigma_{sgl}(t)$ is a monotonically decreasing function of time. Times between the breakdown of the DLR and the onset of the PLR fall into the IR. The quantities on the R.H.S. of eqs A2.1 and A2.2 were obtained utilizing BFMC data in the PLR as indicated in Table 3. For this purpose the data were fit with

$$\sigma_{dbl}(t) = A_{dbl} + B_{dbl}\log(\log t) \quad (A2.3)$$

$$\sigma_{sgl}(t) = A_{sgl}(\log t)^{B_{sgl}} \quad (A2.4)$$

which provide a good description of $\sigma_{sgl}(t)$ and $\sigma_{dbl}(t)$ in the PLR. The needed time derivatives for A2.1 and A2.2 were obtained analytically from the fits.

Appendix 3. We find that the rates of single-chain adsorption and loop formation scale with the fraction of available sites written generally as

$$R \propto f_A^{\beta} = \left(1 - \frac{\sigma_{occ}}{\sigma_{max}}\right)^{\beta} \quad (A3.1)$$

We introduce a reduced (scaling) variable $\sigma^* = \sigma_{occ}R_g^2$ yielding

$$R \propto f_A^{\beta} = \left(1 - \frac{\sigma^*}{R_g^{\,2}\sigma_{max}}\right)^{\beta} \quad (A3.2)$$

For σ^* to be a valid scaling variable, $R(\sigma^*,L_i) = R(\sigma^*,L_j)$, or

$$\left(1 - \frac{\sigma^*}{R_{g,i}^{\,2}\sigma_{max}}\right)^{\beta_i} = \left(1 - \frac{\sigma^*}{R_{g,j}^{\,2}\sigma_{max}}\right)^{\beta_j} \quad (A3.3)$$

where L_i, $R_{g,i}^2$, and β_i correspond to the chain length of chains of type i. For $\sigma^*/R_{g,j}^2\sigma_{max} \ll 1$, or equivalently, $\sigma_{occ} \ll \sigma_{max}$, expansion yields

$$\frac{\beta_i}{R_{g,i}^{\,2}} = \frac{\beta_j}{R_{g,j}^{\,2}} \quad (A3.4)$$

LA051750V